Solid State Sciences 148 (2024) 107410

Contents lists available at ScienceDirect

Solid State Sciences

journal homepage: www.elsevier.com/locate/ssscie

A facile solid state synthesis route to tantalum oxynitride, β-TaON

Jessica C. McGlynn [a], M. Davide Cappelluti [a], James M. Hanlon [a,1], Sina Saremi-Yarahmadi [a,b], Nicolás Flores-González [a], Duncan H. Gregory [a,*]

[a] West-CHEM, School of Chemistry, University of Glasgow, Glasgow, G12 8QQ, UK
[b] Department of Materials, Loughborough University, Loughborough, LE11 3TU, UK

ARTICLE INFO

Keywords:
Synthesis
Tantalum
Nitride
Oxynitride
Photocatalyst
Structure

ABSTRACT

Tantalum oxynitride is a prospective pigment and has attracted considerable recent attention as a photocatalyst for the overall splitting of water under visible light irradiation. Conventionally, TaON is synthesised by the thermal ammonolysis of Ta_2O_5, a process which remains challenging to scale up. The use of ammonia/water or ammonia/oxygen within a narrow temperature window is required to produce high purity TaON material; otherwise Ta_3N_5 forms as the favoured ammonolysis product. It would be highly beneficial to develop a reliable, simpler and reproducible synthesis route to TaON without the use of gaseous ammonia under such complex conditions. This paper describes a facile synthesis route to monoclinic β-TaON (space group $P2_1/c$) using Ta_3N_5 itself as a *solid state* nitrogen source. After 6 h of reaction at 900 °C under vacuum followed by post-synthesis calcination at 580 °C for 30 min, the bright yellow oxynitride is produced as spherical particles *ca.* 80 nm in diameter with a direct band gap of 2.9 eV.

1. Introduction

Traditionally, inorganic materials chemists have focused on manipulating the cation sub-latices of solids (e.g. through substitution, intercalation etc) as a primary means to modify structure and to tune physical and chemical properties. Increasingly, however, solid state chemistry research has turned to the role of anions and the transfer of many of the established materials design concepts to creating mixed anion or heteroanionic materials. These approaches have sparked great interest since both exotic and beneficial properties can be found in heteroanionics that do not exist in single anion compounds. This presents the solid state chemist with new territory for materials discovery and new vistas for materials synthesis [1]. Of the growing classes of heteroanionic materials in existence, oxide nitrides (sometimes termed oxonitrides or oxynitrides) have proved worthy of study on account of a host of physical and chemical properties with important potential real-world applications, including uses as visible light photocatalysts, pigments and magnetic materials [2–4].

The tantalum-oxygen-nitrogen system is a very interesting case in point and the ternary phase field contains compounds with properties that are suited to both their employment as pigments and photocatalysts. Tantalum nitride, Ta_3N_5 (orthorhombic, space group *Cmcm*) was first isolated in 1937 during the decomposition of the tantalum trichlorodiamide heptammine, $Ta(NH_2)_2Cl_3(NH_3)_7$ (itself formed from the action of liquid ammonia on $TaCl_5$) [5]. The pentanitride is more commonly prepared, however, by the thermal ammonolysis of $TaCl_5$ or of the equivalent Ta(V) oxide, Ta_2O_5 at temperatures as high as 850 °C (where the ammonia decomposition products N_2 and H_2 should predominantly exist) [6,7]. However, the use of ammonia can lead to aggregates of particles in powders or grains of $\geq$*ca.* 500 nm in films with outcomes sensitive to gas flow rate, heating times and precursor morphology [8,9]. Surface area can be difficult to control with adverse implications for catalytic activity that are even less ideal for photocatalysts since the charge carriers are more likely to recombine when migrating over relatively large distances [10,11]. The complete substitution of oxygen for nitrogen (from Ta_2O_5 to Ta_3N_5) results in a significant upward shift of the valence band edge when compared to the Ta(V) oxide, resulting in a change in colour from white Ta_2O_5 to bright, brick red Ta_3N_5 powder and a large decrease in the band gap energy, E_g, from 3.9 to 2.1 eV (Fig. 1) [12].

Tantalum oxynitride, TaON is, to date, the only known ternary compound in the Ta–O–N system. The formation of TaON is effectively achieved by the substitution of three O^{2-} anions in Ta_2O_5 by two N^{3-} anions, whilst maintaining the highest valence state of tantalum at +5.

* Corresponding author.
E-mail address: Duncan.Gregory@Glasgow.ac.uk (D.H. Gregory).
[1] Current address: Ricardo, 18 Blythswood Square, Glasgow, G2 4BG, UK.

https://doi.org/10.1016/j.solidstatesciences.2023.107410
Received 3 November 2023; Received in revised form 8 December 2023; Accepted 11 December 2023
Available online 15 December 2023

Monoclinic, β-TaON is the most stable polymorph and the ideal Baddeleyite (ZrO_2)-type structure contains fully ordered anions with each oxygen atom bonded to three tantalum atoms, while each nitrogen atom is connected to four tantalum atoms. (Ta is thus coordinated by seven anions in total) [13–15]. The valence band in TaON originates predominantly from N(O) 2p orbitals and the conduction band from Ta 5d orbitals, but the hybridisation of the anion 2p orbitals and Ta 5d orbitals resulting from the rather covalent Ta-(O,N) bonds leads to a significant dispersion of the valence band when compared to Ta_2O_5, enabling a shift of the valence band maximum by *ca* 1 eV and consequently a visible light response (Fig. 1) [12,15]. Correspondingly, β-TaON is green/yellow in colour, with a band gap of 2.4 eV. In terms of photo(electro)catalysis, the electronic structure of TaON is a highly promising characteristic, particularly for the splitting of water, since the valence and conduction band edges lend themselves to operation under visible light (400–700 nm). By comparison, the wider band gap of Ta_2O_5 (corresponding to an absorption edge of *ca*. 330 nm) allows it to function only under UV light. The ability to efficiently utilise the majority of the solar energy spectrum for overall water splitting is a key requirement for photocatalysts, as the visible region accounts for approaching 50% of the solar spectrum and the photoconversion efficiency increases significantly as higher wavelengths are absorbed [16].

However, TaON has proven to be a material that is difficult to synthesise in a controlled, reproducible way and high purity can be challenging to achieve. The oxynitride is effectively an intermediate in the synthesis of Ta_3N_5 from Ta_2O_5 and given its relatively low thermodynamic stability, tends to spontaneously proceed to yield Ta_3N_5 once formed in an atmosphere of flowing ammonia gas [7]. It is therefore extremely difficult to isolate by the conventional thermal ammonolysis of Ta_2O_5 and requires strict control of heating/cooling rates and of the flow rate of ammonia. Most commonly, the oxynitride is prepared by utilising a flow of (moist) ammonia (at a reported optimum flow rate of 20 mL min^{-1}) at 800 or 850 °C for 15 h [17,18]. These stringent conditions are essential to achieve high phase purity and to prevent the formation of Ta_3N_5.

The practical difficulties associated with the above synthesis coupled with both the trials of phase purity and the control of O:N ratios in the product have long encouraged synthetic solid state chemists to find an alternative reaction path to TaON. Solid state routes are particularly attractive since they can remove the requirement of "moist" ammonia and in principle offer a much greater level of stoichiometric control (since the nitrogen source need not be in excess). Given the narrow temperature window for TaON formation (higher temperature leads to Ta_3N_5), there is also little opportunity to form dense, crystalline materials to minimise the grain boundaries that promote charge carrier recombination in semiconductors. Ideally, high purity, high surface area nanocrystals of TaON would be preferred for photo(electro)catalytic applications. There have been a small number of successful attempts to synthesise TaON in the solid state and each has considered replacing gaseous ammonia with a solid state nitrogen source. Originally, urea was utilised to provide nitrogen in reactions with Ta_2O_5 in a pseudo-solid state analogy to the ammonolysis process. The urea reactant, added as a solid, would decompose on heating *in situ* to generate ammonia, which in turn reacts with Ta_2O_5 to exchange anions and presumably displace water [19], although a recent study in the GaN-ZnO system suggests that nitridation using urea is achieved *via* cyanamide-type intermediate species [20]. A more recent study replaced urea with the melamine-derived oligomer, melon, $(C_6N_9H_3)_n$, which was proposed to produce both NH_3 and C_2N_2 on its thermal decomposition to convert Ta_2O_5 to TaON [21]. Interestingly, at high temperature TaON appeared to decompose to Ta_2O_5 and TaN rather than form Ta_3N_5, presumably as a result of the relatively low partial pressure of NH_3 (N_2/H_2) in the reaction. Finally, guanidine carbonate was utilised as a nitrogen source in a reaction with $TaCl_5$, but this led to formation of both the β- and γ-TaON polymorphs simultaneously and a possible contamination with Ta_2O_5 [22]. In similarity to the previous synthesis methodology, the likely reaction mechanism is proposed to also involve the decomposition of (intermediate) melon (to NH_3 and C_2N_2) and the subsequent reaction with $TaCl_5$.

In this paper we describe a very different approach to TaON synthesis and present a reaction that occurs exclusively in the solid state; a true solid state synthesis of TaON. The reaction itself requires neither gaseous ammonia (or water) nor decomposition of a solid state nitrogen source and is performed under controlled, entirely repeatable reaction conditions. The process is a simple solid state combination of the two binary compounds, Ta_2O_5 and Ta_3N_5.

2. Experimental

2.1. Ta_3N_5 synthesis

The oxide precursor powder, Ta_2O_5 (Strem, 99.8%) was ground using a mortar and pestle until a homogeneous powder was obtained. The powder was placed in an alumina boat inside a horizontal tube furnace which was initially purged with dry argon gas. The sample was subsequently heated at 850 °C at a rate of 5 °C min^{-1} for 12 h under a

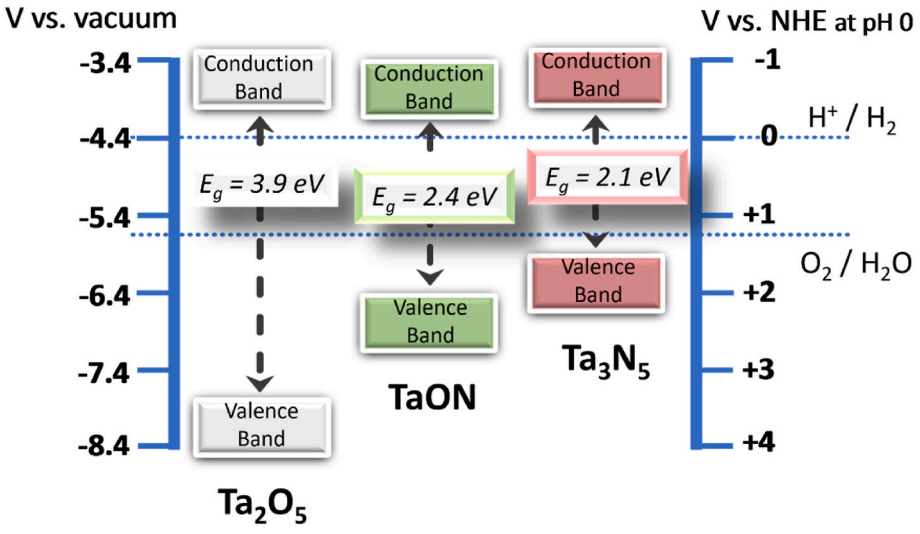

Fig. 1. Schematic of the shift in valence band maximum to higher energy with increasing nitrogen content. The potentials for hydrogen and oxygen reduction are shown for reference.

flow of dry ammonia gas (BOC, 99.98%; 50 mL min^{-1}). The furnace was subsequently switched off under an ammonia flow and the sample was left to cool to ambient temperature before its removal, having first, again, purged the tube furnace with a flow of dry argon gas.

2.2. TaON synthesis

Samples of as-prepared Ta_3N_5 (synthesised as described above) were mixed with Ta_2O_5 (Strem, 99.8%) in oxide/nitride molar ratios between 1:1 and 0.95:1 using a mortar and pestle. The ground, homogenous powder was then sealed in a quartz tube under vacuum and heated to 900 °C for 6 h at a heating rate of 5 °C min^{-1}. After heating, the resultant green powdered products were annealed in air at 580 °C (5 °C min^{-1} heating rate) for 30 min to obtain bright yellow powders.

A "control" sample of TaON was also synthesised using a traditional ammonolysis method employing moist ammonia gas. In this preparation, pre-ground Ta_2O_5 (Strem, 99.8%) powder was placed in an alumina boat within a tube furnace that was initially purged with argon. The sample was heated to 800 °C at a rate of 5 °C min^{-1} for 12 h under a flow of ammonia gas (BOC, 99.98%) that was first bubbled through a Dreschel bottle of distilled water [17]. The furnace was subsequently switched off under the ammonia/water flow and the sample was left to cool to ambient temperature. The tube furnace was purged with a flow of dry argon gas prior to the sample's removal.

2.3. Materials characterisation

Powder X-ray diffraction (PXD) data for the products and reactants were collected using a PANalytical X'pert Pro MPD diffractometer with Cu-$K_{\alpha 1}$ radiation (1.5406 Å) in Bragg-Brentano reflection geometry between $5 \leq 2\theta/^\circ \leq 85$ for approximately 1 h, with a step size of 0.016° and a monochromator slit width of 10 mm. Extended scan times of 3–5 h were used to collect data suitable for Rietveld refinement. Rietveld refinement against PXD data was performed using the GSAS software package through the EXPGUI user interface [23,24].

Scanning Electron Microscopy (SEM) images were obtained using a Phillips XL30 ESEM instrument working in high vacuum mode with an applied accelerating voltage of 25 kV and a working distance of 5 mm for the imaging of sample morphology and particle size measurements. EDS measurements (coupled with SEM) were performed using an Oxford Instruments X-act spectrometer. The EDS spectrometer was calibrated using the INCA EDX software with Cu as the calibration standard. A working distance of 10 mm was employed for EDS measurements. Samples were mounted on adhesive carbon tabs placed on aluminium stub sample holders.

Raman spectroscopy was performed by using a Horiba-Jobin Yvon LabRAM HR confocal microscope (Horiba Ltd., Kyoto, Japan) system with a variable optical hole aperture (100–300 μm) 600 mm^{-1} grating and a Synapse CCD detector. The excitation source was a Nd:YAG second harmonic laser (Ventus532, Laser Quantum, emission $\lambda = 532$ nm, output power 50 mW–1.5 W). The spectra were collected over an effective Raman shift range of 10–1000 cm^{-1}. Laser intensity was tuned from 1 to 25% of the maximum power, preventing *in situ* modification (heating) of the samples (e.g. phase transformations).

C,H,N combustion microanalysis was performed using an EAI Exeter Analytical CE-440 Elemental Analyser with each sample (*ca.* 5 mg) measured in duplicate. Nitrogen physisorption experiments for determination of specific surface area (by the BET method) and pore analysis were conducted using a Quadrasorb EVO ODS-30. Samples (*ca.* 0.1 g) were outgassed at 673 K under flowing N_2 prior to analysis. Helium was used as a calibrant and nitrogen as the absorbent at 77 K. The particle sizes and distributions in solution were assessed by Dynamic Light Scattering (DLS) using a Malvern Panalytical Zetasizer instrument.

Simultaneous thermogravimetric-differential thermal analysis (TG-DTA) was conducted using a Netzsch STA 409 instrument contained within an Ar-filled MBraun UniLab recirculating glovebox (O_2 and H_2O < 0.1 ppm) coupled to a Hiden HPR20 mass spectrometer. Accurately weighed samples of 15–30 mg were heated in alumina crucibles under a constant flow of Ar (BOC, ≥99.999%, 60 mL min^{-1}) at a heating rate of 5 °C min^{-1} to a maximum temperature of 1000 °C. Samples were then left to dwell isothermally for 60 min before cooling to room temperature.

The optical band-gaps of samples were determined using diffuse reflectance UV-Vis (DR-UV-Vis) spectroscopy (Shimadzu UV-2700 equipped with an integrating sphere; ISR-2600 Plus, Shimadzu, Japan). $BaSO_4$ (Nacalai Tesque, Japan) was used as a reference for both absorbance and reflectance measurements. The spectra were recorded at room temperature in a wavelength range of 190–1300 nm.

3. Results and discussion

3.1. Synthesis of Ta_3N_5

Ta_3N_5 was prepared as a single phase by the thermal ammonolysis of Ta_2O_5 as described in the experimental section. The Ta_3N_5 obtained was a bright brick red powder and identified by PXD by comparison to the entry for Ta_3N_5 in the ICDD database (PDF card no: 01-079-1533) (Fig. S1). All diffraction peaks could be assigned to Ta_3N_5. Rietveld Refinement against the PXD data resulted in the expected pseudo-Brookite structure (orthorhombic; space group *Cmcm*) with lattice parameters of $a = 3.891(2)$ Å, $b = 10.222(5)$ Å and $c = 10.276(6)$ Å, which are in close agreement to the reported literature values (allowing for differences in measurement temperature) [6,25]. A refinement profile plot, crystallographic data and bond distances/angles for the synthesised Ta_3N_5 material are presented in the supplementary information (Fig. S2; Tables S1–S3).

The obtained sample of Ta_3N_5 powder was composed of agglomerations of approximately spherical particles, as can be seen in Fig. S3. Each individual particle is of the order of 50–100 nm across. The porous appearance of the particles is perhaps indicative of voids/channels caused by the formation and release of water as oxide is exchanged for nitride in the bulk of the material (Equation (1)). Similar porosity was originally observed in 2004 when the ammonolysis of Ta_2O_5 was first identified as a pseudomorphic and topotactic process [18]. The porosity in this earlier study was proposed to be a consequence of the replacement of 3 oxide anions by 2 nitride anions, although it should be noted that the cation:anion ratio in the structures is also modified by the change in cation stoichiometry. The higher density of Ta_3N_5 results in an inevitable volume decrease on its formation from the pentoxide.

$$3\ Ta_2O_5 + 10\ NH_3 \rightarrow 2\ Ta_3N_5 + 15H_2O \quad (1)$$

Although PXD suggests that the ammonolysis product is single phase (all peaks can be attributed to Ta_3N_5), in previous studies, oxygen has been found to be a ubiquitous impurity in the synthesis of the nitride, especially when synthesised from a Ta_2O_5 precursor, leading to substitutional defects predominantly at the three-coordinate anion site in the Pseudo-Brookite structure [25,26]. Therefore, we considered it important to confirm the composition and stoichiometry of the nitride material and this was achieved using a combination of EDS at the (sub) micron scale and microanalysis of the bulk powder. The tantalum and nitrogen content was calculated over several particle clusters in the sample by EDS (Table S4). Although the EDS spectra suggest no presence of oxygen (supplementary information; Fig. S4), differentiating between the O and N spectral lines can be challenging. CHN microanalysis in fact intimated a lower nitrogen content than was detected by EDS and the difference was assumed to be due to the presence of oxygen in the sample (Table S5). Combining the EDS and microanalysis results and assuming no vacancies, the molecular ratios of Ta, N and O could be estimated. The wt.% (at.%) of Ta and the amount of nitrogen were determined from EDS data and microanalysis, respectively (supplementary information; Tables S4 and S5). The remainder of the anion

content quantified from EDS was then attributed to oxygen. These measurements led to a formula of "$Ta_{2.9(1)}N_{4.8(1)}O_{0.8(2)}$". The implications are either that the Ta_3N_5-type phase is slightly deficient in nitrogen (and could contain both substituted and interstitial oxide) or that the sample contains an undetectable (perhaps X-ray amorphous) fraction of remaining Ta_2O_5. The structural model from Rietveld refinement against PXD data and the ensuing interatomic distances and angles (supplementary information) are in excellent agreement with previous reports on Ta_3N_5 and not surprisingly using X-ray methods, the model could not be improved by replacing (isoelectronic) N^{3-} by O^{2-} on the anion sites (or by attempting to place additional O on empty interstitial sites). The final model therefore contains nitrogen at 100% occupancy across the 3 available anion sites.

3.2. Synthesis of TaON

The proposed reaction to form TaON is expressed in Equation (2):

$$Ta_2O_5 + Ta_3N_5 \rightarrow 5\ TaON \quad (2)$$

The subsequent 1:1 solid state reaction of Ta_2O_5 and Ta_3N_5 resulted in the formation of a green powdered product of nominal TaON. PXD diffractograms indicated a match to the ICDD entry for TaON but also revealed the presence of a low level of tantalum(V) oxide impurity, which could originate directly from the Ta_2O_5 starting material and/or from the presence of oxygen in the Ta_3N_5 precursor (as highlighted in the analysis of the nitride presented above). This issue could be overcome by varying the ratio of reactant oxide, Ta_2O_5 to nitride, Ta_3N_5. It was found that by increasing the nitride content (corresponding to an oxide:nitride ratio of 0.95) the synthesis resulted in the formation of a dark green product, which could again be assigned principally to TaON in diffractograms. Nevertheless, powder patterns revealed such samples contained a small amount of residual Ta_3N_5. Previous TG-DSC experiments had revealed that Ta_3N_5 is fully oxidised to Ta_2O_5 by heating in air at temperatures above approximately 630 °C [8]. We therefore explored annealing under milder conditions in an effort to remove Ta_3N_5 without full oxidation of the entire material to Ta_2O_5. Subsequent annealing of the dark green powder in air at 580 °C for 30 min resulted in the formation of bright yellow TaON with the same monoclinic structure as the green powders and no further evidence of Ta_3N_5 (or any other) impurity. The flat background seen in powder patterns of the annealed material would also suggest the absence of any amorphous by-products. Very similar results have previously been observed from annealing and were considered essential to obtain single phase material [17]. Fig. 2 shows the PXD pattern of the phase-pure yellow material. We subsequently performed a TG-DTA experiment (supplementary information) with a mixture of Ta_2O_5 and Ta_3N_5 under flowing argon (to mimic the inert synthesis conditions as closely as possible). The DTA data informed us that an exothermic reaction occurs with an onset temperature of *ca.* 800 °C. From the TGA profile, there is a negligible mass loss (<0.5 wt%) associated with this process up to the maximum measured temperature of 1000 °C. Mass spectra collected as a function of time/temperature show no evolution of nitrogen, ammonia, oxygen, hydrogen or water. The data are thus consistent with an exothermic solid state reaction of the oxide and nitride to TaON.

The Raman spectrum for annealed TaON is shown in Fig. 3 and compared to the equivalent spectrum for the same sample prior to annealing and to a spectrum taken for the "control" (wet ammonia synthesis) sample of TaON. Group theory predicts 15 IR-active modes ($8A_u + 7B_u$) and 18 Raman-active modes, which are given by the representations $9A_g + 9B_g$. Of the Raman-active modes, those at 178, 258, 415, 527, 660, 759 and 808 cm^{-1} are proposed to be longitudinal optical (LO) modes and their overtones [27]. It has been claimed previously for Ta_2O_5 that the bands in the low/mid-frequency range (100-450 cm^{-1}) correspond to O–Ta–O bending modes in TaO_6 octahedra whereas higher frequency vibrations (450–900 cm^{-1}) arise from coupled Ta–O stretching modes [28]. The assignment of bands in TaON is likely to follow a similar pattern and the Raman spectra of the 3 samples are in many respects identical, with only subtle differences evident. There is an almost imperceptible red shift in the position of the bands in annealed TaON (and in the unannealed sample) compared to the control sample. Nevertheless, this shift would be consistent with increased oxygen content in yellow TaON compared to the control. There is also evidence of additional weak intensity bands in the 200–250 cm^{-1} and 300–350 cm^{-1} regions in the spectrum of the control sample. These weak bands occur in regions that are not predicted (for example, by DFPT/PBE methods) to contain Raman active modes for TaON [27]. It is feasible that the peaks between 200 and 250 cm^{-1} could originate from the active A_g and B_g modes of Ta_3N_5. The low intensity peak(s) in the 300–350 cm^{-1} region, however, do not match convincingly with bands for either Ta_3N_5 or Ta_2O_5 [27,28].

SEM images of annealed TaON are shown in Fig. 4. The images suggest agglomerates of asymmetric but approximately spherical

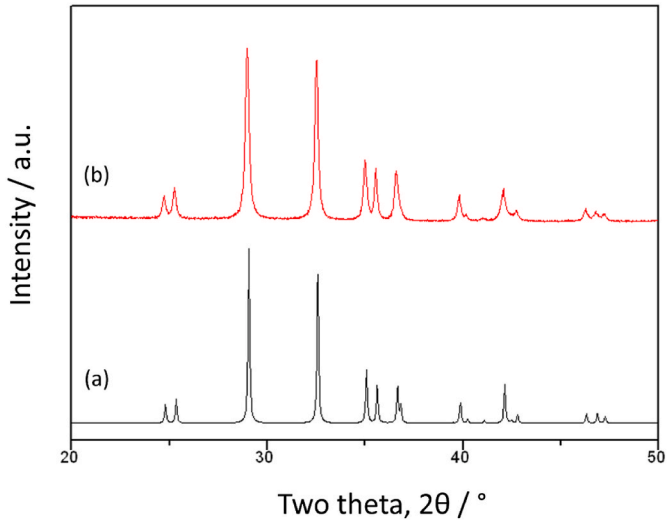

Fig. 2. PXD patterns of: (a) TaON as calculated from the ICSD database, card number 98662 and (b) TaON formed after solid state reaction and post-synthesis annealing at 580 °C for 30 min.

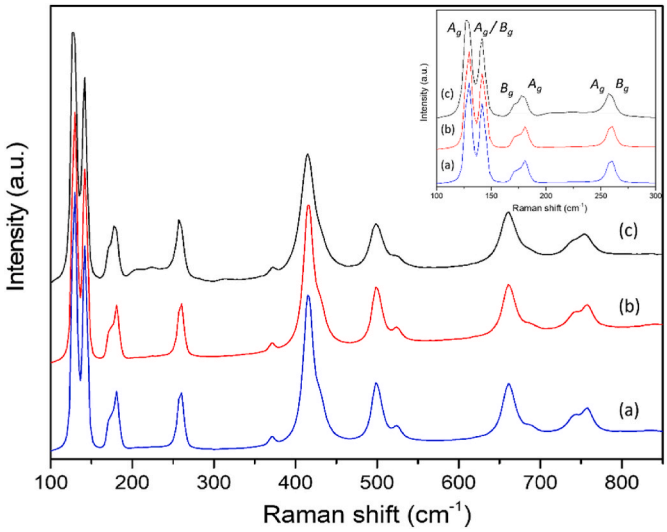

Fig. 3. Raman spectra of: (a) annealed (yellow) TaON; (b) TaON formed directly after solid state reaction (prior to post-synthesis annealing at 580 °C for 30 min); (c) the "control" sample of TaON synthesised using a flow of moist ammonia. The inset shows a magnification of the low Raman shift region with assigned bands labelled.

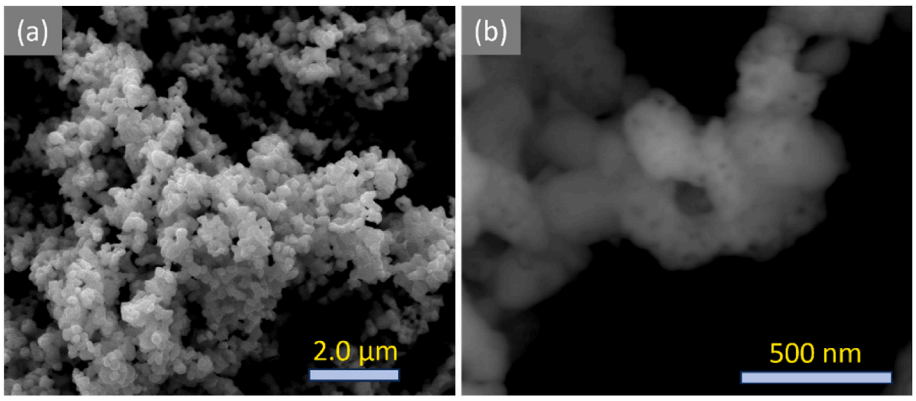

Fig. 4. SEM micrographs of TaON at (a) low magnification (x15000) showing clusters of approximately spherical, sub-micron sized particles; (b) higher magnification (x100000), illustrating the apparent porosity within agglomerated particles.

particles approximately 80 nm in diameter. The particles bear evidence of irregularly distributed, macro/meso-scale pores comparable to those witnessed in the Ta_3N_5 precursor. As for the synthesis of Ta_3N_5 from Ta_2O_5, the conversion of Ta_2O_5 to TaON by ammonolysis has been previously reported to be pseudomorphic and topotactic [18]. From our evidence, the solid state formation of TaON would also appear to be a pseudomorphic one. Despite the presence of pores, the BET surface area of annealed TaON is rather low, with a measured value of 8.43(1) m^2g^{-1} obtained. Prior to the annealing step, the dark green material (containing low level Ta_3N_5 impurity) registered a surface area of 7.67(1) m^2g^{-1}. By comparison, a surface area of the same order, yet slightly higher - 10.85(1) m^2g^{-1} - was obtained for the Ta_3N_5 nitride precursor. From previous literature evidence, it is apparent that the use of reaction temperatures as high as 900 °C has routinely led to rather mediocre BET surface areas for TaON [18]. Our measurements demonstrate that both Ta_5N_5 and annealed TaON describe a Type II BET isotherm (see supplementary information for the isotherm of the latter; Fig. S5). The BET profiles suggest both samples are macroporous and given the relatively low surface areas, each is close to the non-porous regime [29]. In solution, although there is no apparent decomposition, DLS results would tend to suggest that TaON and Ta_3N_5 materials have a tendency to agglomerate (Supplementary Information; Fig. S6). Scattering profiles for annealed TaON as compared to the Ta_3N_5 starting material and the control sample of green TaON synthesised by the traditional "moist ammonia" thermal synthesis technique were rather comparable. Each delivered a monomodal particle size distribution with peak particle diameters across the 100s of nm range (Yellow TaON: 468 ± 23 nm; Ta_3N_5: 538 ± 35 nm; Control TaON: 693 ± 25 nm).

EDS and CHN microanalysis were performed on samples of both as-synthesised and annealed TaON in order to determine the cation and anion stoichiometry of the materials. Tables of the microanalysis data, EDS results and a representative spectrum are shown in the supplementary information (Tables S6–7; Fig. S7). From the combined analyses, the as-synthesised (dark green) and annealed (yellow) materials were found to be oxygen-rich to various degrees, yielding compositions of "$TaO_{1.06(2)}N_{0.90(2)}$" and "$TaO_{1.21(2)}N_{0.84(2)}$", indicating that the annealed material in particular is non-stoichiometric and defective. The excess of oxygen in the yellow oxynitride is most likely to originate from the post-synthesis annealing step which was used to purify the sample. In this case it is feasible that oxide from air displaces nitride (in a reverse process of the ammonolysis of Ta_2O_5, or TaON). Another possible source of the excess oxygen could be from the solid state and may result from the use of a Ta_3N_5 precursor that itself apparently contained more oxygen than expected ("$Ta_{2.9}N_{4.8}O_{0.8}$"). This was previously manifested in our 1:1 reaction mixtures producing Ta_2O_5 impurities in the TaON products as noted above. Niobium – present as "NbO_xN_y" - has also been postulated as a significant impurity in TaON in the literature, since 5 ppm or more of the metal oxide, Nb_2O_5 is often found in Ta_2O_5 and when ammoniated, "NbO_xN_y" is claimed to be (partly) responsible for the green colour of TaON [17]. Nb content below EDS detectable limits could lead to overestimates of the oxygen content in our materials, since the O stoichiometry is deduced by difference on the assumption of no other impurities within the samples. In fact, annealed TaON has a composition similar to other TaON materials reported in the literature, including, for example, $TaO_{1.24}N_{0.84}$ [30] which has a comparable PXD pattern and is also apparently phase-pure. Previous TEM/SAED investigations suggested that $TaO_{a>1}N_{b<1}$ intermediates with monoclinic superstructures (which might perhaps be approximated to $TaO_{1+y}N_{1-y}$) crystallise during the progressive ammonolysis of Ta_2O_5 to TaON [31]. These species were not previously observable by PXD, however, and similarly we see no evidence of superstructure reflections in our diffractograms. The formation of anion defects in TaON appears to be a stable process, especially in layers close to the surface [32]. This argument follows a similar line to that used for Ta_3N_5 where computational studies have indicated that O impurities (in the form of *anti*-site, substitutional defects, O_N) stabilise the nitride structure relative to nitrogen vacancies (V_N) widening the valence band and increasing the mechanical stability of the solid (compared to both nitrogen-poor and stoichiometric Ta_3N_5) [26]. We will return to the issue of stoichiometry when we consider the optical band gaps of TaON below.

Mindful of the results from elemental analyses, Rietveld refinement was performed against PXD data taken for the phase-pure yellow TaON. Based on results from EDS and microanalysis, our starting model was based on non-stoichiometric $TaO_{1.2}N_{0.8}$ and compared to a parallel refinement using a basis of stoichiometric TaON. Both these models assume that the oxidation state of Ta is (very close to) +5, consistent with the colour of the material, and the estimation that for "TaO_aN_b" $2a + 3b \approx 5$ (which yields $TaN_{0.84}O_{1.24}$ from N analysis results). Both refinements employed the monoclinic structure of TaON with only the population of the anion sites distinguishing them apart. The refinements otherwise followed conventional strategies in which global/instrumental parameters (e.g. scale factor, background coefficients, cell parameters etc) were varied first, followed by peak width/shape parameters and concluding with atomic parameters (positions, thermal displacement parameters etc.). Inevitably, due to the limitations of light elements to scatter X-rays (and the inability to distinguish between nominal O^{2-} and N^{3-} adequately), the oxygen and nitrogen occupancies could not be refined to convergence and were subsequently fixed at 1.0 for the oxygen (O1) site and to 0.8:0.2 for O:N on the nitrogen (N2) site (or to 1.0 N on the N2 site in the stoichiometric model). The quality of the fit (R-factors and errors) was found to be slightly improved in the non-stoichiometric model when compared to stoichiometric TaON.

From Rietveld refinement, therefore, $TaO_{1.2}N_{0.8}$ crystallises in the monoclinic $P2_1/C$ space group as per stoichiometric TaON. Crystallographic data, atomic parameters and selected interatomic distances and angles for $TaO_{1.2}N_{0.8}$ are presented in Tables 1–3 and the corresponding

Table 1
Crystallographic data for annealed TaON from Rietveld refinement against PXD data at 298 K.

Radiation	X-ray
Wavelength, λ/Å	Cu-$K_{\alpha 1}$; 1.5406
Chemical Formula	$TaO_{1.2}N_{0.8}$
Formula Mass/g mol^{-1}	848.291
Crystal System	Monoclinic
Space Group	$P2_1/c$
a/Å	4.968 (2)
b/Å	5.036(3)
c/Å	5.184(3)
B/°	99.6(1)
Cell Volume/$Å^3$	127.87(2)
Z	4
Calculated density, ρ_X/g cm^{-3}	11.016
No of data	8377
No of Parameters	41
R_{wp}	0.091
R_P	0.072
Goodness of fit, χ^2	2.32

Table 2
Atomic parameters for $TaO_{1.2}N_{0.8}$ from Rietveld refinement against PXD data at 298 K.

Atom Type	Site	x	y	z	U_{iso}/$Å^2$	Site Occupancy
Ta	4*e*	0.292 (1)	0.045 (1)	0.216 (1)	0.947 (3)	1.0
O1	4*e*	0.06(2)	0.32(1)	0.34(1)	2.24(2)	1.0
O2	4*e*	0.45(3)	0.74(2)	0.48(3)	2.24(2)	0.2
N2	4*e*	0.45(3)	0.74(2)	0.48(3)	2.24(2)	0.8

Table 3
Selected interatomic distances (Å) and angles (°) for $TaO_{1.2}N_{0.8}$ from Rietveld refinement against PXD data at 298 K.

Interatomic distances/Å	
Ta–O1	1 × 2.013(6)
	1 × 2.034(13)
	1 × 2.173(6)
Ta-(N2,O2)	1 × 2.034(13)
	1 × 2.118(12)
	1 × 2.124(11)
	1 × 2.127(12)
Ta–Ta	2 × 3.241(7)
	2 × 3.316(6)
	1 × 3.321(12)
Interatomic angles/°	
O1–Ta–O1	1 × 104.7(3)
	1 × 148.4(3)
(N2,O2)–Ta–(N2,O2)	1 × 99.5(5)
	1 × 136.5(7)

refinement profile plot is shown in Fig. 5. Lattice parameters of a = 4.968(2) Å, b = 5.036(3) Å, c = 5.184(3) Å and β = 99.6(1) ° were obtained leading to a slightly increased cell volume as compared to literature values for stoichiometric TaON from neutron and synchrotron X-ray diffraction [15]. The structure of TaON has been previously described in detail in the literature but contains a single seven-fold Ta environment and two anion environments that are three- (O1) and four-coordinate (N2), respectively. From our structural model, the mean cation-anion bond length is 2.07(1) Å to the former three-coordinate anion position and 2.10(1) Å for the latter. This further reinforces the premise that the lower coordination number site is occupied by oxide and the latter predominantly occupied by nitride both from the respective ionic radii and by consideration of the mean bond lengths in Ta_3N_5 and Ta_2O_5 [27,33].

The optical band gaps of selected TaON samples were determined

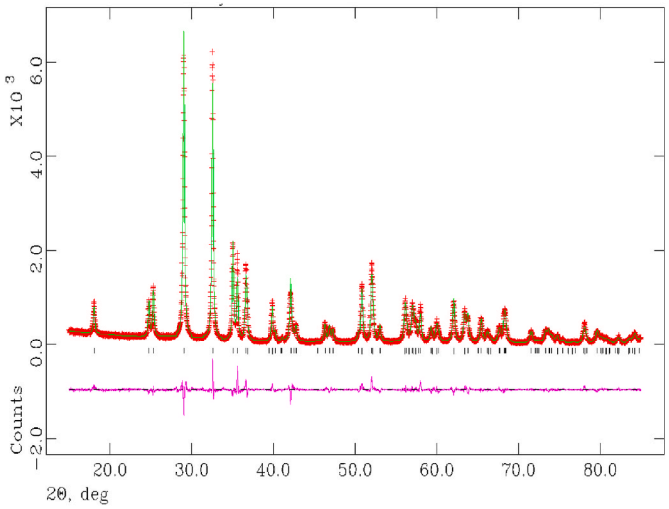

Fig. 5. Observed (red), calculated (green) and difference (magenta) profile plot for the refinement against PXD data for annealed TaON. Black vertical markers show the Bragg reflections from the $TaO_{1.2}N_{0.8}$ phase.

using UV-Vis Diffuse Reflectance Spectroscopy, as seen in Fig. 6. Several independently synthesised samples of annealed TaON were measured for an evaluation of consistency. The results were compared with measurements taken from control samples of TaON (prepared via wet ammonia synthesis). From the Tauc plots, we can determine that the direct band gap of yellow $TaO_{1.2}N_{0.8}$ is 2.87 ± 0.05 eV, which is somewhat higher than the 2.44 eV reported by Density Functional Theory [34]. Interestingly, the direct band gap of the control sample is the same within error; 2.88 ± 0.03 eV. The indirect band gaps of the annealed and control materials are entirely different, however, with the latter significantly smaller than the former; 2.66 ± 0.05 eV for $TaO_{1.2}N_{0.8}$ vs. 2.36 ± 0.03 eV for the control TaON material. Given that the annealed, yellow oxynitride is non-stoichiometric and rich in oxide, it is reasonable to assume that this higher oxygen content has an influence on the valence band position (and shape). The increased oxygen content, present as anti-site defects, O_N, acts so as to limit the shift upwards of the valence band maximum on replacement of O^{2-} by N^{3-}, yielding E_g values intermediate between the 3.9 eV and 2.4 eV gaps of Ta_2O_5 and TaON respectively.

The negative connotations of a wider gap were borne out in preliminary photocatalytic tests that we performed using $TaO_{1.2}N_{0.8}$ in the degradation of methylene blue (supplementary information; Fig. S8). Tests demonstrated that although the material was indeed photocatalytically active in visible light, the degradation rates were slow when compared to some Ta_3N_5 materials, unsurprisingly especially those doped with ruthenium, or those employing other co-catalysts or promoters [10,35,36]. Significant improvements would need to be made to solid state synthesied TaON materials in order to make them more competitive as photocatalysts for dye degradation or water splitting; surface area is rather low, defects could act as trapping centres and the surface chemistry needs to be understood and optimised such that catalysts might be effectively activated. Nevertheless, there is significant inherent scope in the method for sensitive band gap control through O:N stoichiometric tuning (*via* Ta_2O_5:Ta_3N_5 ratios). For non-catalytic applications, such as solid state pigments, this might be sufficiently useful for further materials development given that the brightness can also be improved on annealing. The synthesis experiments have also emphasised that the purity/stoichiometry of the starting nitride is likely to be pivotal in prescribing colour and that the post-synthesis annealing could be crucial in honing the surface activity for catalysis. Although proving effective in improving phase purity, air (oxygen) annealing may well deactivate the catalyst and annealing under nitrogen or nitrogen/hydrogen (as has often been undertaken for nitrogen-transfer

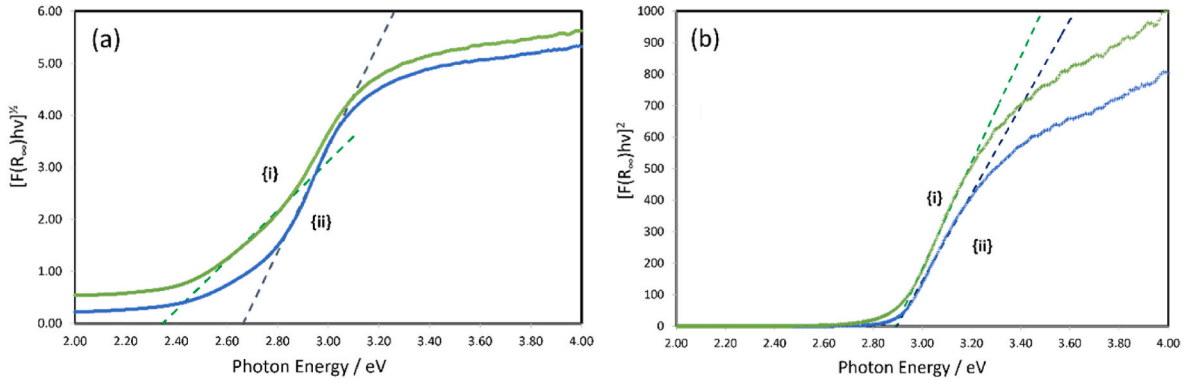

Fig. 6. Tauc plots for: (a) allowed indirect transitions and (b) allowed direct transitions calculated from DR-UV-Vis spectra measured for samples of {i} the control TaON synthesised by wet ammonolysis and {ii} annealed TaON ($TaO_{1.2}N_{0.8}$).

catalysts) might prove more effective in shifting towards N-rich compositions (through reduction/anion exchange), changing surface composition and, in turn, improving performance.

4. Conclusions

Monoclinic tantalum(V) oxynitride was successfully synthesised via a new solid state route. The reaction of tantalum oxide and tantalum nitride at 900 °C for 6 h yielded a green TaON product which was then annealed in air to achieve a phase-pure bright yellow material crystallising in monoclinic space group $P2_1/c$. SEM/EDS and microanalysis indicated that the clusters of so-formed spherical nanoparticles of approximately 80 nm in diameter were non-stoichiometric and rich in oxygen, which could be formulated as $TaO_{1.2}N_{0.8}$. Structure refinement against powder X-ray diffraction data intimated that the most likely model invokes anti-site disorder with additional oxygen accommodated on the nitrogen site. UV-Vis Diffuse Reflectance Spectroscopy resulted in direct and indirect band gaps of 2.9 eV and 2.7 eV for the bright yellow $TaO_{1.2}N_{0.8}$. The indirect gap is notably larger than that for TaON prepared by ammonolysis with wet ammonia and the value of E_g can be evidently engineered through manipulating O:N ratios. Although the synthesis resulted in a catalytically active material, photocatalytic performance is unimpressive and further work is required to design higher surface area, nitrogen-rich oxynitrides if photo(electro)catalysis is to be the primary use of these materials.

CRediT authorship contribution statement

Jessica C. McGlynn: Investigation, Visualization, Writing - original draft. **M. Davide Cappelluti:** Formal analysis, Investigation, Visualization. **James M. Hanlon:** Investigation, Supervision. **Sina Saremi-Yarahmadi:** Formal analysis, Investigation, Writing - review & editing. **Nicolás Flores-González:** Formal analysis, Investigation. **Duncan H. Gregory:** Conceptualization, Formal analysis, Funding acquisition, Methodology, Project administration, Supervision, Writing - review & editing.

Declaration of competing interest

The authors declare the following financial interests/personal relationships which may be considered as potential competing interests: Duncan H Gregory reports financial support was provided by European Commission. Duncan H Gregory reports financial support was provided by University of Glasgow. Nicolas Flores Gonzalez reports financial support was provided by National Commission for Scientific and Technological Research. If there are other authors, they declare that they have no known competing financial interests or personal relationships that could have appeared to influence the work reported in this paper.

Data availability

Data will be made available on request.

Acknowledgements

The authors are grateful to the University of Glasgow for a studentship for M.D.C. The research post for J.M.H received funding from the European Union's Seventh Framework Programme (FP7/2007-2013) for the Fuel Cells and Hydrogen Joint Technology Initiative under Grant Agreement number 30344. The authors acknowledge the Advanced Human Capital Program of the National Commission for Scientific and Technological Research (CONICYT/Becas Chile/N° 72170338) for a PhD scholarship for N.F.G.

Appendix A. Supplementary data

Supplementary data to this article can be found online at https://doi.org/10.1016/j.solidstatesciences.2023.107410.

References

[1] H. Kageyama, K. Hayashi, K. Maeda, J.P. Attfield, Z. Hiroi, J.M. Rondinelli, K. R. Poeppelmeier, Expanding frontiers in materials chemistry and physics with multiple anions, Nat. Commun. 9 (2018) 772, https://doi.org/10.1038/s41467-018-02838-4.
[2] M. Ahmed, G. Xinxin, A review of metal oxynitrides for photocatalysis, Inorg. Chem. Front. 3 (2016) 578–590, https://doi.org/10.1039/C5QI00202H.
[3] F. Tessier, F, P. Maillard, F. Cheviré, K. Domen, S. Kikkawa, Optical properties of oxynitride powders, J. Ceram. Soc. Jap. 117 (1361) (2009) 1–5, https://doi.org/10.2109/jcersj2.117.1.
[4] A. Fuertes, Metal oxynitrides as emerging materials with photocatalytic and electronic properties, Mater. Horiz. 2 (2015) 453–461, https://doi.org/10.1039/C5MH00046G.
[5] H. Moureu, C.H. Hamblet, The ammonolysis of tantalum pentachloride, J. Am. Chem. Soc. 59 (1937) 33–40, https://doi.org/10.1021/ja01280a009.
[6] N.E. Brese, M. O'Keeffe, P. Rauch, F.J. DiSalvo, Structure of Ta_3N_5 at 16 K by time-of-flight neutron diffraction, Acta Crystallogr. C47 (1991) 2291–2294, https://doi.org/10.1107/S0108270191005231.
[7] G. Brauer, J. Weidlein, J. Strähle. Über das Tantalnitrid Ta_3N_5 und das Tantaloxidnitrid TaON, Z. Anorg. Allg. Chem. 348 (5–6) (1966) 298–308, https://doi.org/10.1002/zaac.19663480511.
[8] Q. Zhang, L. Gao, Ta_3N_5 nanoparticles with enhanced photocatalytic efficiency under visible light irradiation, Langmuir 20 (2004) 9821–9827, https://doi.org/10.1021/la048807i.
[9] M. Kerlau, O. Merdrignac-Conanec, M. Guilloux-Viry, A. Perrin, Synthesis of crystallized TaON and Ta_3N_5 by nitridation of Ta_2O_5 thin films grown by pulsed laser deposition, Solid State Sci. 6 (2004) 101–107, https://doi.org/10.1016/j.solidstatesciences.2003.10.010.
[10] G. Hitoki, A. Ishikawa, T. Takata, J.N. Kondo, M. Hara, K. Domen, K, Ta_3N_5 as a novel visible light-driven photocatalyst (λ<600 nm), Chem. Lett. 31 (2002) 736–737, https://doi.org/10.1246/cl.2002.736.
[11] K. Maeda, (Oxy)nitrides with d^0-electronic configuration as photocatalysts and photoanodes that operate under a wide range of visible light for overall water splitting, Phys. Chem. Chem. Phys. 15 (2013) 10537–10548, https://doi.org/10.1039/C2CP43914J.

[12] W.-J. Chun, A. Ishikawa, H. Fujisawa, T. Takata, J.N. Kondo, M. Hara, M. Kawai, Y. Matsumoto, K. Domen, Conduction and valence band positions of Ta_2O_5, TaON, and Ta_3N_5 by UPS and electrochemical methods, J. Phys. Chem. B 107 (2003) 1798–1803, https://doi.org/10.1021/jp027593f.
[13] D. Armytage, B.E.F. Fender, Anion ordering in TaON: a powder neutron-diffraction investigation, Acta Crystallogr B30 (1974) 809–812, https://doi.org/10.1107/S0567740874003761.
[14] M. Weishaupt, J. Strähle, V.O.N. Darstellung der oxidnitride, NbON und TaON. Die kristallstruktur von NbON und TaON, Anorg. Allg. Chem. 429 (1977) 261–269, https://doi.org/10.1002/zaac.19774290132.
[15] M. Yashima, Y. Lee, K. Domen, Crystal structure and electron density of tantalum oxynitride, a visible light responsive photocatalyst, Chem. Mater. 19 (2007) 588–593, https://doi.org/10.1021/cm062586f.
[16] R. Abe, Recent progress on photocatalytic and photoelectrochemical water splitting under visible light irradiation, J. Photochem. Photobiol. C Photochem. Rev. 11 (2010) 179–209, https://doi.org/10.1016/j.jphotochemrev.2011.02.003.
[17] E. Orhan, F. Tessier, R. Marchand, Synthesis and energetics of yellow TaON, Solid State Sci. 4 (2002) 1071–1076, https://doi.org/10.1016/S1293-2558(02)01369-9.
[18] D. Lu, G. Hitoki, E. Katou, J.N. Kondo, M. Hara, K. Domen, Porous single-crystalline TaON and Ta_3N_5 particles, Chem. Mater. 16 (2004) 1603–1605, https://doi.org/10.1021/cm0347887.
[19] Q. Gao, C. Giordano, M. Antonietti, Controlled synthesis of tantalum oxynitride and nitride nanoparticles, Small 7 (2011) 3334–3340, https://doi.org/10.1002/smll.201101207.
[20] K. Katagiri, Y. Hayashi, R. Yoshiyuki, K. Inumaru, T. Uchiyama, N. Nagata, Y. Uchimoto, A. Miyoshi, K. Maeda, Mechanistic insight on the formation of GaN: ZnO solid solution from Zn-Ga layered double hydroxide using urea as the nitriding agent, Inorg. Chem. 57 (2018) 13953–13962, https://doi.org/10.1021/acs.inorgchem.8b02498.
[21] K. Ueda, Y. Inaguma, Y. Asakura, S. Yin, New method for the synthesis of β-TaON oxynitride using $(C_6N_9H_3)_n$, Chem. Lett. 47 (2018) 840–842, https://doi.org/10.1246/cl.180265.
[22] S.K. Khore, S.R. Kadam, B.B. Kale, R.S. Sonawane, Sustain. Energy Fuels 4 (2020) 4671–4678, https://doi.org/10.1039/d0se00791a.
[23] A.C. Larson, R.B. Von Dreele, General Structure Analysis System (GSAS), Los Alamos National Laboratory Report LAUR 86-748, Los Alamos National Laboratory, 1994.
[24] B.H. Toby, EXPGUI, a graphical user interface for GSAS, J. Appl. Crystallogr. 34 (2001) 210–213, https://doi.org/10.1107/S0021889801002242.
[25] S.J. Henderson, A.L. Hector, Structural and compositional variations in Ta_3N_5 produced by high-temperature ammonolysis of tantalum oxide, J. Solid State Chem. 179 (2006) 3518–3524, https://doi.org/10.1016/j.jssc.2006.07.021.
[26] J. Wang, J. Feng, L. Zhang, Z. Li, Z. Zou, Role of oxygen impurity on the mechanical stability and atomic cohesion of Ta_3N_5 semiconductor photocatalyst, Phys. Chem. Chem. Phys. 16 (2014) 15375–15380, https://doi.org/10.1039/c4cp00120f.
[27] E. Nurlaela, M. Harb, S. Gobbo, M. Vashishta, K. Takanabe, Combined experimental and theoretical assessments of the lattice dynamics and optoelectronics of TaON and Ta_3N_5, J. Solid State Chem. 229 (2015) 219–227, https://doi.org/10.1016/j.jssc.2015.06.029.
[28] P.S. Dobal, R.S. Katiyar, Y. Jiang, R. Guo, A.S. Bhalla, Raman scattering study of a phase transition in tantalum pentoxide, J. Raman Spectrosc. 31 (2000) 1061–1065, https://doi.org/10.1002/1097-4555(200012)31:12<1061::AID-JRS644>3.0.CO;2-G.
[29] C. Sangwichien, G.L. Aranovich, M.D. Donohue, Density functional theory predictions of adsorption isotherms with hysteresis loops, Colloids Surf. A Physicochem. Eng. Asp. 206 (2002) 313–320, https://doi.org/10.1016/S0927-7757(02)00048-1.
[30] G. Hitoki, T. Takata, J.N. Kondo, M. Hara, H. Kobayashi, K. Domen, An oxynitride, TaON, as an efficient water oxidation photocatalyst under visible light irradiation (λ≤500 nm), Chem. Commun. (2002) 1698–1699, https://doi.org/10.1039/B202393H.
[31] D. Lu, J.N. Kondo, M. Hara, T. Takata, K. Domen, Systematical investigation on characteristics of a photocatalyst: tantalum oxynitrides, Microscopy 63 (4) (2014) 313–324, https://doi.org/10.1093/jmicro/dfu019.
[32] T. Liu, Q. Zhang, Q. Zhao, Theoretical insight into the anion vacancy healing process during the oxygen evolution reaction on TaON and Ta_3N_5, Phys. Chem. Chem. Phys. 24 (2022) 13999–14006, https://doi.org/10.1039/D2CP01615J.
[33] N.C. Stephenson, R.S. Roth, The crystal structure of the high temperature form of Ta_2O_5, J. Solid State Chem. 3 (1971) 145–153, https://doi.org/10.1016/0022-4596(71)90018-1.
[34] H. Ullah, A.A. Tahir, S. Bibi, T.K. Mallick, S. Zh Karazhanov, Electronic properties of β-TaON and its surfaces for solar water splitting, Appl. Catal., B 229 (2018) 24–31, https://doi.org/10.1016/j.apcatb.2018.02.001.
[35] S.S.K. Ma, T. Hisatomi, K. Maeda, Y. Moriya, K. Domen, Enhanced water oxidation on Ta_3N_5 photocatalysts by modification with alkaline metal salts, J. Am. Chem. Soc. 134 (2012) 19993–19996, https://doi.org/10.1021/ja3095747.
[36] Y. Jiang, P. Liu, Y. Chen, Z. Zhou, H. Yang, Y. Hong, F. Li, L. Ni, Y. Yan, D. H. Gregory, Construction of stable Ta_3N_5/g-C_3N_4 metal/non-metal nitride hybrids with enhanced visible-light photocatalysis, Appl. Surf. Sci. 391 (2017) 392–403, https://doi.org/10.1016/j.apsusc.2016.04.094.